Optoelectronic control of spin dynamics at near-THz frequencies in magnetically doped quantum wells

R. C. Myers,[1] K. C. Ku,[2] X. Li,[2] N. Samarth,[2] and D. D. Awschalom[1]

[1]*Center for Spintronics and Quantum Computation, University of California, Santa Barbara, CA 93106.*
[2]*Department of Physics and Materials Research Institute, The Pennsylvania State University, University Park, Pennsylvania 16802.*

(Dated: February 2, 2008)

We use time-resolved Kerr rotation to demonstrate the optical and electronic tuning of both the electronic and local moment (Mn^{2+}) spin dynamics in electrically gated parabolic quantum wells derived from II-VI diluted magnetic semiconductors. By changing either the electrical bias or the laser energy, the electron spin precession frequency is varied from 0.1 to 0.8 THz at a magnetic field of 3 T and at a temperature of 5 K. The corresponding range of the electrically-tuned effective electron g-factor is an order of magnitude larger compared with similar nonmagnetic III-V parabolic quantum wells. Additionally, we demonstrate that such structures allow electrical modulation of local moment dynamics in the solid state, which is manifested as changes in the amplitude and lifetime of the Mn^{2+} spin precession signal under electrical bias. The large variation of electron and Mn-ion spin dynamics is explained by changes in magnitude of the $sp-d$ exchange overlap.

PACS numbers: 75.50.Pp, 78.47.+p, 85.35.Be, 71.70.Gm

The drive towards quantum information processing using semiconductors has motivated several recent experiments that use high sensitivity time-resolved optical techniques to demonstrate the electrical control of coherent electron spin dynamics in non-magnetic III-V semiconductor heterostructures.[1] Proof-of-concept experiments have exploited variations in the spin-orbit interaction due to quantum confinement in a heterostructure,[2] compositional gradients,[3] and epitaxial strain.[4] The energy of these effects in conventional semiconductors, however, is on the μeV scale and is manifested as variations in the spin precession frequency in the GHz range. In contrast, THz electron spin precession frequencies are easily achieved in magnetic semiconductors because the Hamiltonian includes the $s-d$ exchange interaction which leads to giant spin splittings in the conduction band states on the 10 - 100 meV energy scale.[5] Demonstration of electrically-tunable spin precession in the GHz-THz regime would provide an important advance towards the addressing of quantum states at higher frequencies than currently possible in conventional semiconductors.

Previous work has demonstrated that magnetic doping of II-VI quantum wells (QWs) can be used to engineer the exchange overlap between electron/hole wave functions and local moments (Mn^{2+} ions).[6] This leads to large enhancements of the electron spin precession frequencies and the observation of Mn^{2+} spin precession.[7] Recently, photoluminescence (PL) measurements in conventional III-V QWs with a proximal ferromagnetic barrier have also revealed that a bias voltage may be used to tune the spin coupling between carriers in the QW and the ferromagnetic layer; however spin dynamics could not be measured in these structures.[8] Here, we demonstrate the optoelectronic tuning of electron spin precession frequency from the GHz to near-THz regime in electrically biased, magnetically-doped II-VI parabolic quantum wells (PQWs). Electrical bias also modifies the local moment (Mn^{2+}) spin dynamics indicating a change in the magnetic-ion and hole exchange overlap. Large variations in the electron spin dynamics occur as a function of the excitation laser energy due to changes in the occupation of states in the PQWs. Tuning of the $sp-d$ exchange overlap between the Mn^{2+} and the electron and hole wave functions is therefore demonstrated using both electrical bias and laser excitation energy.

The samples are grown by molecular beam epitaxy (MBE) and consist of 100 nm ZnSe /50 or 100 nm PQW/500 nm ZnSe/ (001) n+GaAs wafer. The optically active region consists of a ZnSe-$Zn_{0.85}Cd_{0.15}Se$ PQW in which the concentration of Cd is graded using digital shuttering with a 2.5 nm period for the 50 nm sample (Sample 1) and a 5 nm period for the 100 nm sample in order to achieve a parabolic band edge profile,[9] as shown schematically in Fig. 1a. Mn doping is performed using digital shuttering such that four 1/8 monolayers of MnSe are deposited within a 5 nm region at the center of each well. Control samples of both 50 nm width (Sample 2) and 100 nm width containing no Mn doping are also grown. A vertical electrical bias (V_b) is applied between a transparent front gate of evaporated Ti/Au and the n+GaAs substrate.

PL is measured normal to the sample surface as a function of magnetic field (B) in both Voigt (optical axis $\perp B$) and Faraday (optical axis // B) geometries under fixed vertical bias (Fig. 1b). The excitation consists of linearly polarized light from a pulsed laser at an energy of 2.88 eV, power density of 56 W/cm^2, and with a ~ 50 μm average spot diameter. Gaussian fits to the quantum well PL peaks are used to extract intensity, emission energy, and linewidth as a function of magnetic field for a variety of vertical biases (Fig. 1c). The Mn-doped 50 nm PQW (sample 1) shows a large Zeeman shift of ~ 20 meV for

magnetic fields between 0 T and 6 T in the Faraday geometry and ~ 10 meV in the Voigt geometry, whereas the corresponding control (sample 2) shows < 0.3 meV shift. The larger shift in Faraday versus Voigt geometry for the magnetic sample is attributed to the lifting of the valence band degeneracy due to quantum confinement. In the Faraday case, heavy hole ($j = 3/2$) spins are pinned out of plane leading to larger spin splitting than in the Voigt geometry.[10] We have observed PL energy shifts of up to 2 meV due to V_b in both the magnetic and non-magnetic PQW (compare closed symbols to open symbols in Fig. 1c). However, precision measurement of these shifts is hampered by the rapid quenching of the PL intensity and the linewidth broadening observed under vertical bias.

Spin dynamics are measured by time-resolved Kerr rotation (KR) in the Voigt geometry with the optical path parallel to the growth axis.[7] A Ti:Sapphire laser with a 76 MHz repetition rate and ~ 150 fs pulse width is split into a 1 mW pump beam and a 0.2 mW probe beam. The helicity of the pump beam polarization is modulated at 50 kHz by a photo-elastic modulator, while the intensity of the linearly polarized probe beam is modulated by optical chopper at 1 kHz for lock-in detection. The

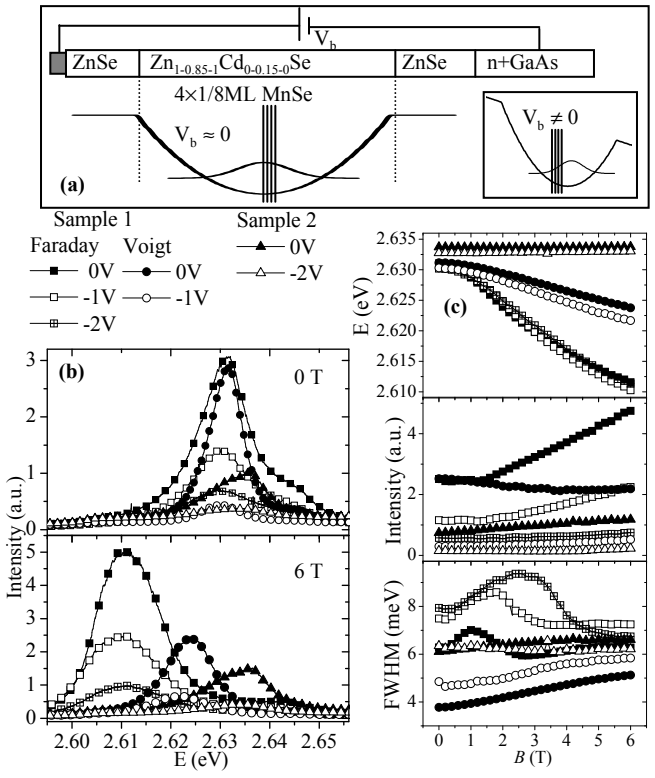

FIG. 1: (a) Schematic of sample structure (not to scale), electrical wiring, conduction band edge and ground state electron wave function. The inset illustrates wave function spatial translation under vertical bias. (b) Photoluminescence of 50 nm Mn-doped (Sample 1) and 50 nm control (sample 2) at 5 K and $B = 0$ T (top) and 6 T (bottom) under various V_b. (c) PL emission energy (E), intensity, and FWHM extracted from Gaussian fits to PL as a function of E.

pump and probe beams are focused to an overlapping $\sim 50\mu$m diameter spot on the sample, which sits in a magneto-optical cryostat with a split-coil superconducting magnet.

We measure the rotation of the axis of polarization (θ_K) of the reflected probe beam as a function of time (Δt) using an optical delay line in the path of the probe beam. In this geometry, angular momentum is injected parallel to the sample growth axis and perpendicular to the magnetic field at $\Delta t = 0$, resulting in a spin precession about the applied field. In magnetically doped samples, both a short lived electron spin precession and a long lived Mn^{2+} spin precession are observed. The latter precession originates from an effective tipping field due to the $p-d$ interaction between the short-lived photoinjected spin-polarized holes and the paramagnetically aligned Mn^{2+} spin.[7] The data can be fit to two exponentially decaying cosines with the Kerr rotation expressed as, $\theta_K(\Delta t) = A_e e^{(-\Delta t/T^*_{2e})} cos(2\pi\nu_e \Delta t + \phi_e) + A_{Mn} e^{(-\Delta t/T^*_{2Mn})} cos(2\pi\nu_{Mn}\Delta t + \phi_{Mn})$, where A_e (A_{Mn}) is the amplitude of electron (Mn^{2+}) spin precession, T^*_{2e} (T^*_{2Mn}) is the transverse electron (Mn^{2+}) spin lifetime, ν_e (ν_{Mn}) is the electron (Mn^{2+}) spin precession frequency, and ϕ_e (ϕ_{Mn}) is a phase offset. The precession frequencies are expressed in terms of effective g-factors, $\nu_e = g_e \mu_B B/h$, and $\nu_{Mn} = g_{Mn}\mu_B B/h$, where g_e and g_{Mn} are the effective g-factors for electron and Mn^{2+} spin respectively, μ_B is the Bohr magneton, and h is Planck's constant.

Figure 2a plots Kerr rotation as a function of both vertical bias and time delay for Sample 1 at 5 K and $B =$ 3 T with a pump-probe energy (E_p) of 2.638 eV. Two distinct spin precession components are observable and the parameters extracted from fits to the data (Fig. 2b) are presented in Fig. 2c-e. The short-lived component is attributed to electron spin, and reveals large tuning of the precession frequency ($g_e = 1.6$ to 8.4) with vertical bias, while the long-lived component is attributed to Mn^{2+} spin precession whose frequency remains constant ($g_{Mn} = 2.0240 \pm 0.0006$ fit precision, not systematic error).

Several observations indicate that a spatial translation of the electron wave function due to vertical bias occurs in both the magnetic and non-magnetic samples. The non-magnetic sample (sample 2) reveals the expected g-factor tuning due to the Cd concentration gradient (inset of Fig. 2c) and an increase in T^*_{2e} under negative bias. Both these effects have been observed in non-magnetic GaAs-AlGaAs III-V PQW, where the g-factor tuning was attributed to the spatial translation of the electron wave function into regions of increased Al concentration and the increase in lifetime was attributed to the electron and hole separation (splitting of the exciton) with bias.[3] For the magnetic sample at zero bias, where we would expect maximum overlap with the Mn layers, we observe the maximum electron g-factor and minimum T^*_{2e}, while negative bias leads to a decrease in g_e and an increase in T^*_{2e}. These changes reflect the fact that $s-d$ overlap both

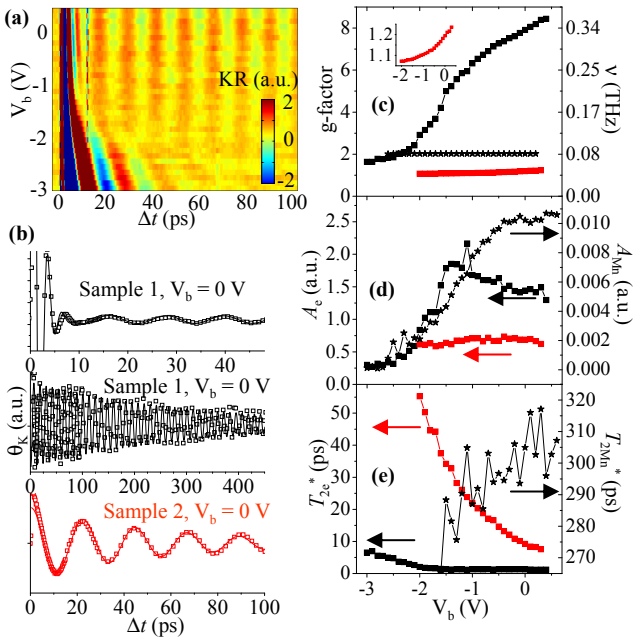

FIG. 2: (color) (a) KR of sample 1 as a function of V_b and Δt at 5 K and $B = 3$ T. (b) KR as a function of Δt at fixed V_b. Raw data (squares) and fits (lines) are plotted in three panels: (top) sample 1 at short Δt fit to two decaying cosines for both electron and Mn-ion spin precession, (middle) sample 1 at long Δt fit to a single decaying cosine for Mn spin precession only, and (bottom) sample 2 fit to a single decaying cosine for electron spin precession only. (c) Spin precession frequency and effective g-factor (inset: sample 2 data enlarged to show non-magnetic g-factor tuning due to Cd concentration gradient), (d) amplitude, and (e) lifetime are plotted as a function of V_b. Sample 1 data are black points with squares (stars) for electron (Mn) parameters and sample 2 data are red squares.

increases the electron spin splitting and enhances electron spin scattering, noting that T_{2e}^* is larger in the non-magnetic sample over the bias range measured. Qualitatively identical vertical biasing effects are observed in another Mn-doped 50 nm PQW with 1 nm period thickness, and in the 100 nm Mn-doped PQW, where the effective electron g-factor tunes from 2 to 14 (data not shown), thus demonstrating the reproducibility of $s-d$ enhanced g-factor tuning in II-VI PQW.

The vertical bias also leads to a spatial translation of the hole wave function, and is manifested by changes in the Mn^{2+} spin dynamics. At zero bias, the Mn^{2+} spin precession amplitude (A_{Mn}) and the spin lifetime (T_{2Mn}^*) are at a maximum, while negative bias leads to a decrease in both quantities. As mentioned earlier, the Mn^{2+} spin precession is triggered by an effective magnetic tipping pulse applied to the paramagnetically aligned Mn^{2+} spin by the short-lived spin-polarized holes that are injected at $\Delta t = 0$. At zero bias, the Mn^{2+} spin precession amplitude is large since the hole exchange ($p-d$) overlap and, therefore, the effective tipping field is large; under vertical bias the $p-d$ overlap is decreased such that the tipping field and, therefore, A_{Mn} both decrease. We speculate that the decrease in Mn^{2+} spin lifetime with vertical bias could be due to an increase in the recombination time of photo-excited carriers as a result of splitting the exciton. If the recombination time increases then the temporal cross-section for carrier-Mn spin scattering increases.

We also examine the dependence of the electron spin coherence to the laser pump-probe energy (E_p) and find that the electron spin precession frequency is maximized at the lowest E_p ($g_e \sim 18$ at 2.611 eV), while it saturates for higher E_p ($g_e \sim 6$ at 2.627-2.650 eV), as shown in Fig. 3. Given the magnitude of the electron g-factor shifts due to E_p in comparison to the g-factor tuning due to vertical bias (Fig. 2c), the E_p effect is interpreted as a result of the dependence of the electron and Mn overlap (at the center of the wells) on the sublevel energy within the PQW. Qualitatively, the s-like ground state wave function (probed under the lowest energies) achieves a maximum overlap integral with the Mn^{2+} doped region, whereas excited state wave functions have more widely distributed probability densities and thus overlap less with Mn^{2+} in the center of the wells. This is consistent with the decrease in electron effective g-factor (Fig. 3c) and increase in electron spin lifetime (Fig. 3e) observed under higher pump-probe energy. The electron spin precession amplitude has sharp features when E_p is resonant with the heavy hole exciton lines,[11] which are labeled as $n = 1$ (red line) and $n = 2$ (blue line) in Fig. 3d. These features match the qualitative interpretation described above such that an increasing E_p leads to photo-excited electron occupation of both $n = 1$ and $n = 2$ states resulting in a decreasing g_e. Once E_p is at or above the $n = 2$ energy, g_e saturates because occupation and measurement of $n = 1$ states is unlikely. A quantitative understanding of this effect would require two-color pump-probe measurements.

Due to the large pump-probe energy dependence of the electron spin coherence as presented in Fig. 3, the vertical biasing effects observed for both electron and Mn^{2+} spin coherence in magnetic PQW (Fig. 2) could be interpreted, not as a result of spatial wave function translation as previously discussed, but as due to the quantum confined stark effect[12] (QCSE) redshift of the absorption edge such that, for a given E_p, the application of a vertical bias would lead to higher energy sublevels being probed and therefore a decrease in the effective electron g-factor (Fig. 3). However, a correspondingly large QCSE shift is not observed in the gated PL data (Fig. 1) in which under applied bias we observe a maximum shift of 2 meV in the PL emission energy, while the application of the same bias results in an almost ten-fold decrease in the electron precession frequency. We also note that the largest change in g_e is observed over a ~ 20 meV pump-probe energy range, thus QCSE shifting (≤ 2 meV) is unlikely to be the cause of the change in g_e under vertical bias.

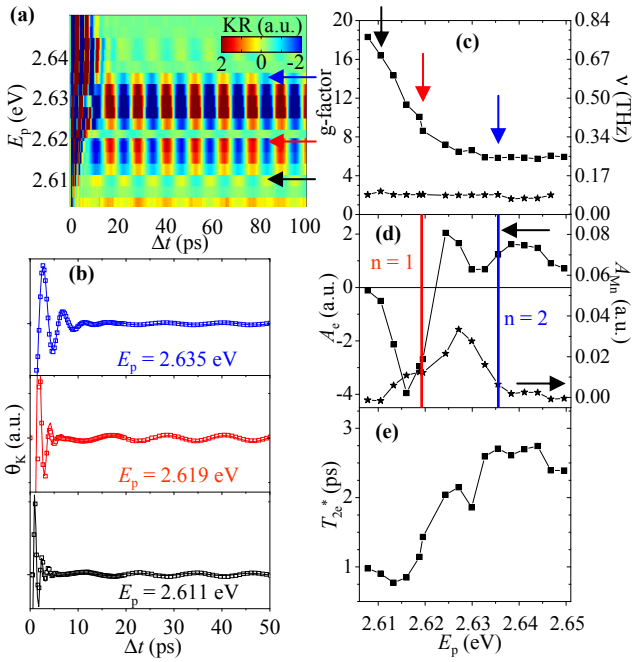

FIG. 3: (color) (a) KR at 5 K and $B = 3$ T of sample 1 as a function of E_p. (b) Line cuts at constant E_p of data from (a), marked by colored arrows, are plotted as a function of Δt. Both raw data (squares) and fits (lines) are presented. (c) Spin precession frequency and effective g-factor, (d) amplitude, and (e) lifetime are plotted as a function of E_p. In part (d) vertical colored lines label features corresponding to heavy hole exciton resonance lines for the ground state ($n = 1$, red line) and first excited state ($n = 2$, blue line).

Our data indicate that both vertical biasing and choice of pump-probe energy can be used to alter electron and Mn^{2+} spin dynamics in a magnetic II-VI PQW. As expected, the large exchange coupling between electron and Mn^{2+} spin in these structures increases the electron g-factor tuning by at least an order of magnitude compared with non-magnetic II-VI or III-V PQW structures. A change in magnitude of the $sp-d$ exchange overlap has been observed to occur due to the spatial translation of the carrier wave functions under vertical bias. The change in electron spin dynamics due to laser energy is also interpreted in the context of exchange overlap, such that higher laser energy probes spatially broader carrier wave functions. In the current symmetric Mn doping scheme, the vertical bias pulls both electron and hole wave functions away from the Mn ions; future structures with asymmetric Mn doping could be envisaged in which the effects of $s-d$ and $p-d$ exchange interaction on the spin dynamics could be separately examined.

Acknowledgments

We thank M. Poggio, Y. K. Kato, J. Berezovsky, A. W. Holleitner, and R. J. Epstein for a critical reading of the manuscript. Work supported by grants NSF-DMR-0305223 and -0305238, DARPA/ONR N0014-99-1-1096 and -1093, AFOSR F49620-02-10036, and ARO DAAD19-01-1-0541.

[1] D. D. Awschalom and N. Samarth, in *Semiconductor spintronics and Quantum Computation*, eds. D. D. Awschalom, D. Loss, and N. Samarth, Springer-Verlag (2002).
[2] M. Poggio, G. M. Steeves, R. C. Myers, N. P. Stern, A. C. Gossard, and D. D. Awschalom, Phys. Rev. B **70**, 121305(R) (2004).
[3] G. Salis, Y. Kato, K. Ensslin, D. C. Driscoll, A. C. Gossard and D. D. Awschalom, Nature **414**, 619 (2001); Y. Kato, R. C. Myers, D. C. Driscoll, A. C. Gossard, J. Levy, and D. D. Awschalom, Science **299**, 1201 (2003).
[4] Y. Kato, R. C. Myers, A. C. Gossard, and D. D. Awschalom, Nature **427**, 50 (2004).
[5] T. Dietl, (Diluted) Magnetic Semiconductors, in Handbook of Semiconductors, (ed. S. Mahajan) Vol.3B (North-Holland, Amsterdam, 1994), p. 1251; D. D. Awschalom and N. Samarth, J. Mag. Magn. Mater. **200**, 130 (1999).
[6] S. A. Crooker, D. A. Tulchinsky, J. Levy, D. D. Awschalom, R. Garcia, and N. Samarth, Phys. Rev. Lett. **75**, 505 (1999).
[7] S. A. Crooker, D. D. Awschalom, J. J. Baumberg, F. Flack, and N. Samarth, Phys. Rev. B **56**, 7574 (1997); S. A. Crooker, J. J. Baumberg, F. Flack, N. Samarth, and D. D. Awschalom, Phys. Rev. Lett. **77**, 2814 (1996).
[8] R. C. Myers, A. C. Gossard, and D. D. Awschalom, Phys. Rev. B **69**, 161305(R) (2004).
[9] R. C. Miller, A. C. Gossard, D. A. Kleinman, and O. Munteanu, Phys. Rev. B **29**, 3740 (1984).
[10] R. W. Martin, R. J. Nicholas, G. J. Rees, S. K. Haywood, N. J. Mason, and P. J. Walker, Phys. Rev. B **42**, 9237 (1990).
[11] S. A. Crooker, D. D. Awschalom, and N. Samarth, IEEE J. Sel. Top. Quantum Electron. **1**, 1082 (1995).
[12] D. A. B. Miller, D. S. Chemla, T. C. Damen, A. C. Gossard, W. Wiegmann, T. H. Wood, and C. A. Burrus, Phys. Rev. Lett. **53**, 2173 (1984).